processes

MDPI

*Article*

# Peak-Regulation Performance of Thermal Power Plants Integrated with Molten Salt and Heat Pump Thermal Energy Storage

**Lihua Cao [1], Jiaojin Xu [1,2], Feng Hou [1] and Pan Li [1,*]**

[1] School of Energy and Power Engineering, Northeast Electric Power University, Jilin 132012, China; xujiaojinneepuedu@163.com (J.X.)
[2] School of Electrical Engineering, Jilin Technology College of Electronic Information, Jilin 132021, China
* Correspondence: lipanneepuedu@163.com

**Abstract**

To alleviate grid peak-shaving pressure from high-penetration renewable energy integration, coupling thermal energy storage (TES) with coal-fired power plants is an effective approach for enhancing operational flexibility. This paper systematically investigates the peak-shaving performance of a coal-fired unit integrated with molten salt storage and heat pump storage systems, focusing on load response characteristics, peak-shaving capability, and the influence of discharge strategies on thermodynamic performance under various rated turbine heat acceptance (THA) conditions. The results indicate that, under identical peak-shaving capacity, the molten salt system exhibits greater storage capacity, which increases with rising THA levels, whereas the heat pump storage capacity remains largely THA-independent. Regarding discharge strategies, replacing high-pressure extraction steam achieves the fastest ramp rate and largest incremental power output, introducing steam into the intermediate-pressure cylinder yields the slowest response but highest round-trip efficiency, and replacing low-pressure extraction steam delivers the smallest peak-shaving capacity and lowest round-trip efficiency. Although TES integration slightly reduces thermal efficiency due to heat exchange losses, this trade-off is justified by significant flexibility improvement, demonstrating clear engineering value for high-renewable grids.

**Keywords:** thermal power unit; molten salt thermal energy storage; heat pump thermal energy storage; peak-regulation capacity; flexibility



Academic Editor: Bo Yang

Received: 16 May 2026
Revised: 27 June 2026
Accepted: 28 June 2026
Published: 4 July 2026



## 1. Introduction

Driven by the "dual carbon" goals [1], China's installed capacity of renewable energy and its power generation have continued to rise. However, constrained by the inherent intermittency and volatility of renewable energy, its large-scale grid integration poses significant challenges to grid stability [2,3]. As the traditional backbone of power supply, coal-fired power units urgently need to complete the transition from electricity supply to flexible regulation in order to smooth out fluctuations in new energy generation. This places higher demands on the variable-load peak-regulation capability of coal-fired power units. Energy storage technology can reconfigure the spatial and temporal distribution of energy supply and demand, and coupling it with thermal power units is an effective pathway to enhance peak-regulation capability [4]. Coupling thermal energy storage technology has been recognized as an effective approach to enhancing the operational flexibility of

conventional coal-fired power plants. In China, in particular, thermal energy storage has been widely regarded as one of the key enabling solutions for the development of modern power systems [5].

Molten salt thermal energy storage technology [6] is regarded as one of the most promising peak-regulation technologies for thermal power plants because of its high heat storage density, stable operation under high-temperature conditions of 500–600 °C, strong compatibility with the main steam parameters of thermal power units, and high thermal conversion efficiency. Compared with pumped hydro storage and compressed air energy storage systems, molten salt thermal energy storage technology offers the advantages of being free from geographical constraints, allowing on-site construction, and possessing high energy storage density. Relative to battery storage and chemical energy storage, it features a longer service life and lower environmental pollution. Owing to its high specific heat capacity and broad temperature-range stability, molten salt has become the preferred medium for large-scale thermal energy storage systems. Similar advanced thermal management concepts have also played a key role in improving the performance of distributed energy systems [7].

In the construction of coupled systems, the selection of molten salt type, the configuration of thermal storage tanks, the design of heat exchangers, and the matching between these components and the operating parameters of the generating unit are key aspects of system design [8,9]. Current research mainly focuses on the thermodynamic performance and economic analysis of different forms of coupled systems. For example, Lin et al. [10] designed multiple coupling strategies, and the results showed that, compared with a standalone coal-fired power unit, the thermodynamic performance of the coupled systems could be significantly improved, with the maximum equivalent round-trip efficiency reaching 48.89%. Wei et al. [11] constructed a thermal energy storage system using main steam as the heat source and found that, under the 50% THA condition, the system could achieve a peak-regulation capacity of 100 MW. Wang et al. [12] proposed four integrated modes for the extraction and return of main steam/reheat steam and systematically evaluated the peak-regulation performance of each mode. Richter et al. [13] proposed a scheme for integrating thermal energy storage equipment into a power plant system to enhance its flexibility. In their study, the Dymola dynamic simulation software was used to simulate a 695 MW subcritical coal-fired unit. The results showed that the steam thermal energy storage scheme led to a reduction of approximately 7% in net power output, while an additional 4.3% of net power could be gained through heat release from a Ruths accumulator.

In addition to molten salt thermal energy storage, coupling with emerging energy storage technologies also provides an important pathway for enhancing the flexibility of thermal power generation. Heat pump energy storage is a large-scale energy storage technology based on a power cycle [14,15]. During the charging stage, an electrically driven heat pump operates through a reverse Carnot cycle to convert electrical energy into thermal energy, which is then stored in molten salt; during the discharging stage, the high-temperature thermal energy stored in the molten salt is converted back into electrical energy. This process upgrades low-grade thermal energy into high-grade thermal energy through thermodynamic compression. Because the coefficient of performance (COP) is always greater than 1, the amount of thermal energy is amplified during the charging process. C. Salomone et al. [16] pointed out that coupling thermal storage with a heat pump can improve the performance of heat pump systems. Owing to its high heat storage density and small temperature fluctuations, molten salt exhibits significant advantages in heat pump heating management. Wang et al. [17] found that, after coupling an electric heat pump with a combined heat and power unit, the minimum power generation load of the unit could be reduced from 300 MW to 150 MW under a specific heating load, thereby

significantly enhancing its peak-regulation capability. Yu et al. [18] introduced a "thermal power storage-heat pump combined thermal storage" mode into a 600 MW unit. The results showed that, under a thermal storage load of 90 MW, the peak-regulation capacity increased by 78.29 MW and the peak-regulation depth increased by 13.04%.

The above studies consistently indicate that coupling molten salt/heat pump thermal energy storage systems not only helps alleviate the safety issues caused by renewable energy grid integration but also can significantly improve the peak-regulation flexibility of thermal power units. However, existing research has predominantly focused on the efficiency of molten salt/heat pump storage systems and the economic analysis of power plant retrofits, while insufficient attention has been paid to the dynamic response characteristics of coupled molten salt storage and heat pump cycles under flexible peak-shaving scenarios. Furthermore, a systematic comparison between the two storage approaches and an in-depth investigation into their adaptability to off-design unit operating conditions remain lacking.

This paper investigates a coupled system integrating a thermal power plant with molten salt thermal energy storage and heat pump thermal energy storage. A mathematical model of the system is established, and the load response time and peak-regulation performance of the energy storage and energy release processes for both thermal energy storage configurations under different thermal loads are systematically analyzed. Furthermore, the effects of different energy storage and release schemes on the system's peak-regulation capability and thermodynamic performance are explored, with the aim of identifying suitable operating strategies for energy storage/energy release.

## 2. System Overview

Figure 1 is a schematic diagram of the heat storage process of the coupled system integrating a thermal power plant with molten salt thermal energy storage and heat pump thermal energy storage. The system includes the thermal power plant section, the molten salt thermal energy storage section, and the heat pump thermal energy storage section. The thermal power plant section adopts a domestic supercritical 600 MW unit. The steam turbine model is N600-24.2/566/566, a condensing steam turbine with one intermediate reheat, two cylinders, and two exhaust flows, with an exhaust pressure of 0.0049 MPa. The regenerative system consists of three high-pressure heaters, four low-pressure heaters, and one deaerator. The molten salt thermal energy storage section includes two solar salt (60% $NaNO_3$-40% $KNO_3$) storage tanks, HOT1 and LOT1, as well as a molten salt heat exchanger (MSHE). The heat pump thermal energy storage section includes two solar salt storage tanks, HOT2 and LOT2, as well as a Brayton heat pump system. Table 1 summarizes the operating temperature range and the thermophysical property parameters of the molten salt used for heat storage. The thermophysical property parameters of Solar Salt are mainly sourced from the NIST Standard [19] Reference Database. The temperature-dependent correlations for density and specific heat capacity refer to recent molecular dynamics simulations and experimental validation [20].

**Table 1.** Operating temperature range and thermophysical property parameters of molten salt.

| Name | Unit | Temperature Dependence | Operating Temperature Range |
|---|---|---|---|
| $c_p$ | J/(kg·K) | $1396.018 + 0.172T$ | 563~833 K |
| $\lambda$ | W/(m·K) | $0.391 + 1.9 \times 10^{-4}T$ | 563~833 K |
| $\rho$ | kg/m$^3$ | $2263.723 - 0.636T$ | 563~833 K |
| $\mu$ | Pa·s | $0.075 - 2.779 \times 10^{-4}T + 3.488 \times 10^{-7}T^2 - 1.474 \times 10^{-10}T^3$ | 563~833 K |

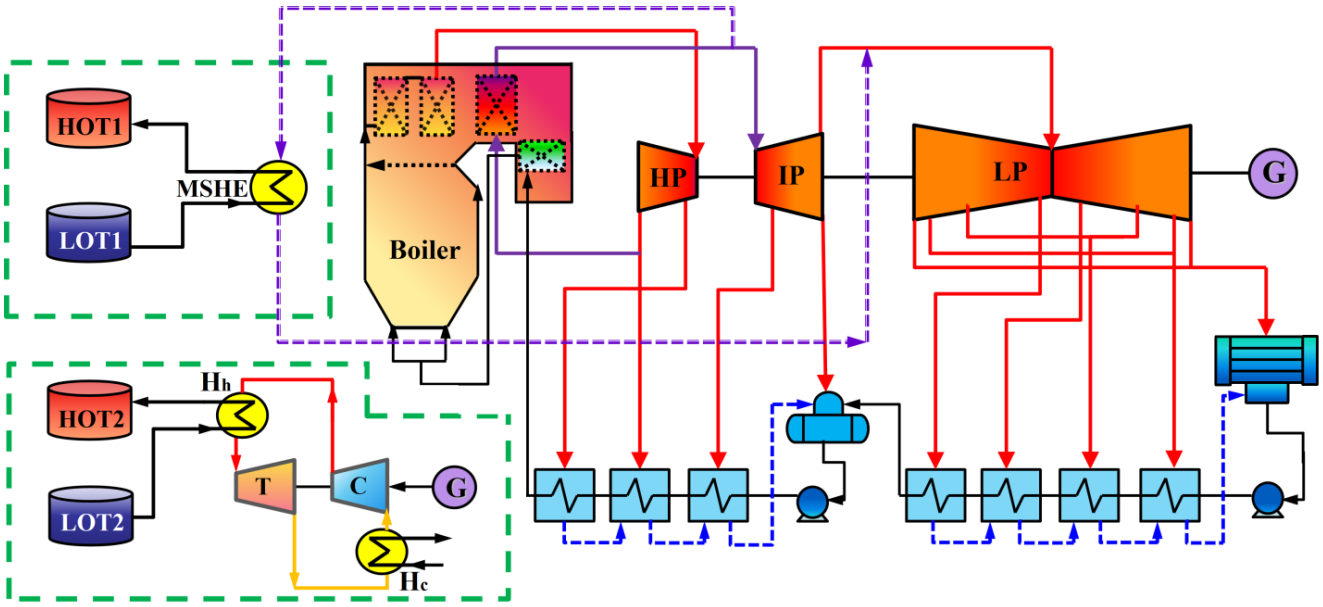


**Figure 1.** Schematic diagram of the heat storage process of the coupled system.

The thermal energy storage process is as follows: as shown in Figure 1, during the molten salt thermal energy storage stage, a portion of the steam at the outlet of the boiler reheater is extracted and exchanges heat with cold molten salt in the MSHE. After the temperature of the molten salt rises, it is stored in HOT1. The steam after heat release is returned to the inlet of the low-pressure cylinder of the steam turbine, and peak regulation is achieved by reducing the steam flow rate doing work in the intermediate-pressure cylinder. In the heat pump thermal energy storage mode, part of the electrical energy generated by the thermal power plant is converted into thermal energy through the Brayton heat pump and stored in the solar salt tank HOT2, and peak regulation is achieved by directly reducing the power output of the unit. The molten salt flow rate is determined by the required thermal storage capacity and the permissible temperature drop across the storage tank. The upper temperature limit is constrained by the thermal decomposition threshold of Solar Salt and is set at 833 K, while the lower limit is constrained by its freezing point and is set at 563 K. This design is consistent with typical practices for compact heat exchangers. During the molten salt thermal energy storage process, in order to ensure the safe operation of the unit, the flow rate of the extracted reheat steam is subject to certain limits. It is necessary to simultaneously ensure that, under the new inlet steam flow rate of the intermediate-pressure cylinder, the overall axial thrust of the steam turbine does not exceed the allowable limit and that the water level of the deaerator does not fall below the safe level. Based on comprehensive considerations, the maximum extraction steam flow rate for molten salt thermal energy storage is determined to be 55 kg/s, which is also the limit of steam extraction of the system and determines the maximum depth of flexible peak regulation for molten salt thermal energy storage. In contrast, the limitations of heat pump thermal energy storage are mainly the safety of its own condenser and the maximum capacity of the solar salt storage tank (that is, the maximum thermal energy storage capacity), which are fewer than those of molten salt thermal energy storage.

Figure 2 shows the schematic diagram of the energy release process of the coupled system. Molten salt thermal energy storage and heat pump thermal energy storage release heat through the surface-type molten salt heat exchangers MSDHE1 and MSDHE2, respectively. After the heat obtained during the storage process is released, it is stored in their respective low-temperature molten salt tanks. In order to better investigate the effects of different extraction and release locations during the energy release process on the coupled

system, three energy release schemes, 1–3, were designed. In Scheme 1, the molten salt heat exchanger is arranged in parallel with four low-pressure heaters to heat the condensate, which is then mixed with the main condensate and enters the deaerator, thereby reducing low-pressure extraction steam, increasing the flow rate through the low-pressure cylinder, and enhancing power output. In Scheme 2, the molten salt heat exchanger is used to heat part of the feedwater extracted from the intermediate tap of the feedwater pump, generating steam that is introduced into the intermediate-pressure cylinder to conduct work, thereby increasing the power output of the intermediate- and low-pressure cylinders. In Scheme 3, the molten salt heat exchanger is arranged in parallel with three high-pressure heaters to heat part of the feedwater, and the heated feedwater is then mixed with the main feedwater and sent into the boiler, thereby reducing high-pressure extraction steam, increasing the flow rate through each cylinder, and rapidly increasing power output. All three energy release schemes can utilize the combined power generation from the boiler and the hot molten salt tank during periods of peak electricity demand.

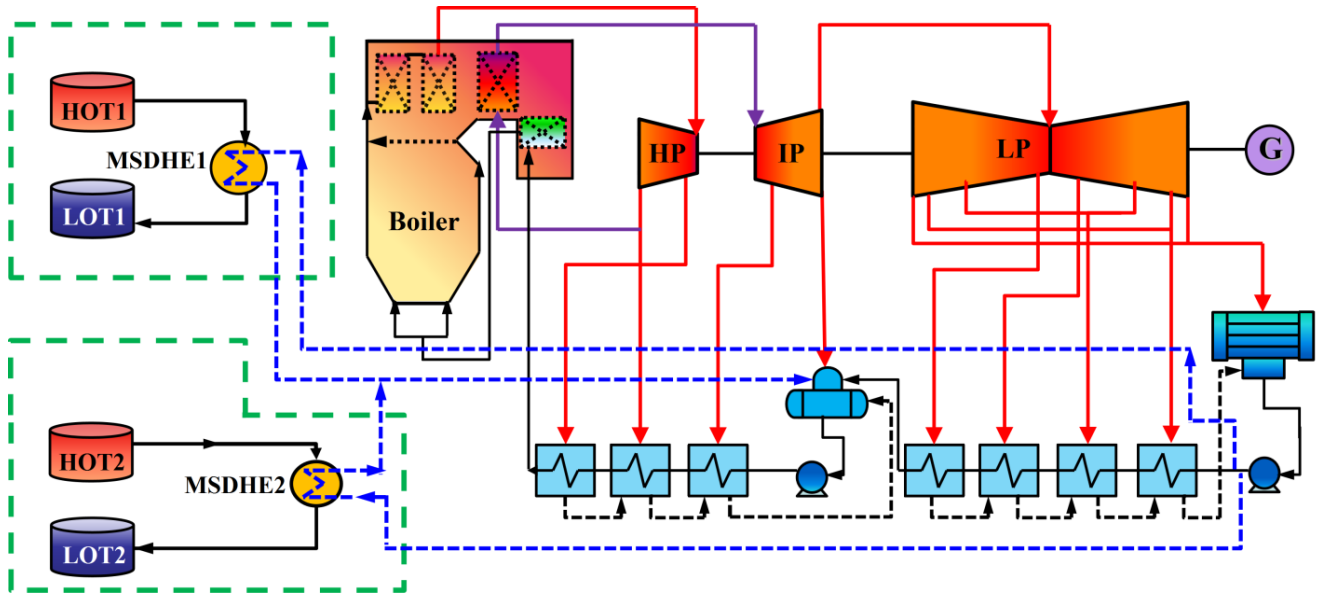


(**a**) Scheme 1

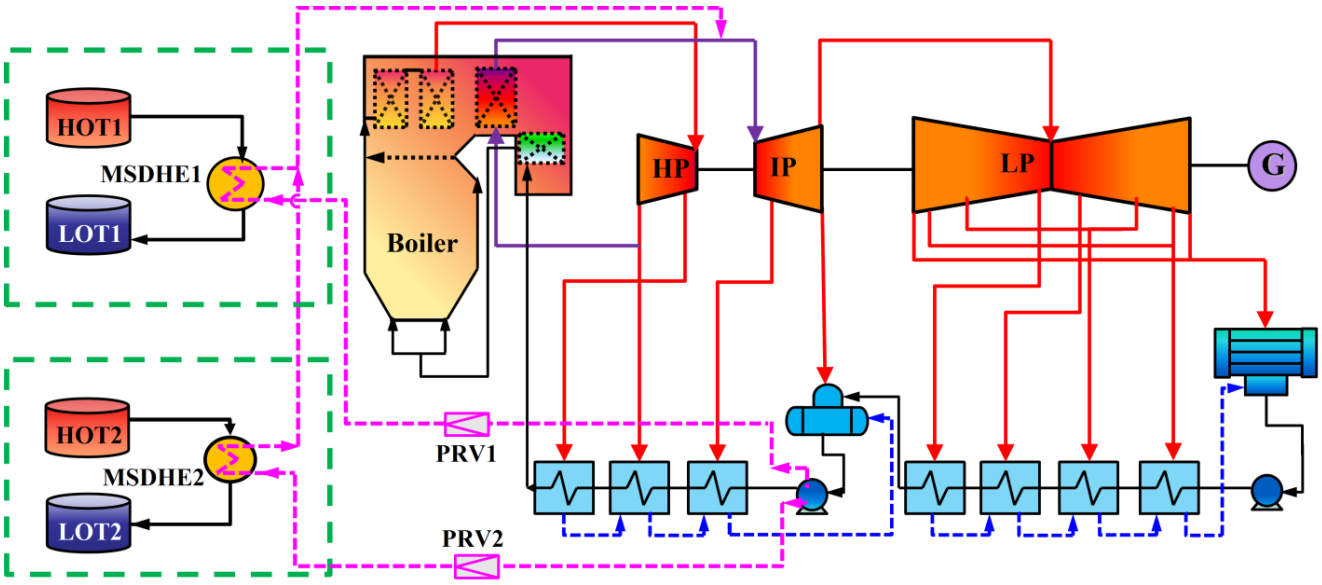


(**b**) Scheme 2

**Figure 2.** *Cont.*

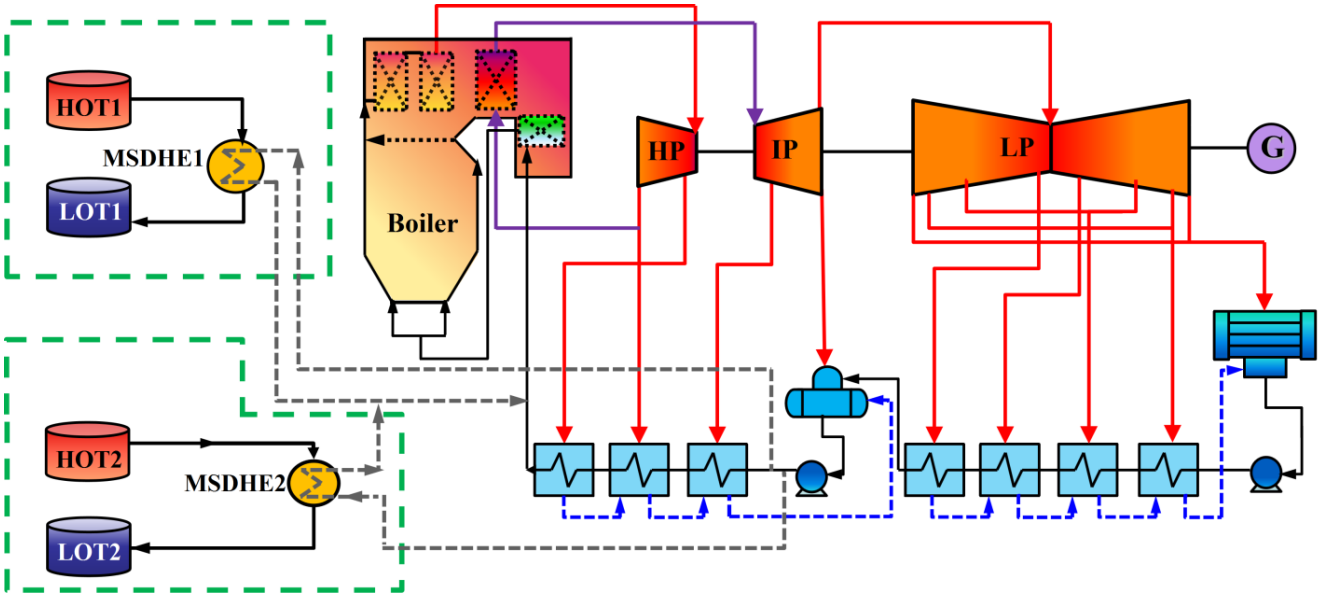


(**c**) Scheme 3

**Figure 2.** Schematic diagram of the heat release process of the coupled system.

## 3. Mathematical Model and Calculation Method

### *3.1. Mathematical Model*

The Brayton heat pump can readily provide high-temperature thermal energy above 400 °C and can be effectively applied in large-scale energy storage. The performance of the heat pump depends on the parameters of its individual components. The working fluid in the heat pump system is initially air, with a cycle pressure ratio of 12.4. Both the compressor isentropic efficiency ($\eta_{\mathrm{comp}}$) and the expander isentropic efficiency ($\eta_{\mathrm{tur}}$) are set to 0.88.

The compressor outlet pressure, outlet temperature, and power consumption are as follows [21]:

$$p_{\mathrm{comp,out}} = \pi p_{\mathrm{comp,in}} \tag{1}$$

$$T_{\mathrm{comp,out}} = T_{\mathrm{comp,in}} \pi^{(n-1)/n} \tag{2}$$

$$W_{\mathrm{comp}} = G_{\mathrm{air}} c_p (T_{\mathrm{comp,out}} - T_{\mathrm{comp,in}}) \eta_{\mathrm{comp}} \tag{3}$$

The turbine outlet pressure, outlet temperature, and power output are as follows:

$$p_{\mathrm{tur,out}} = \pi_{\mathrm{tur}} p_{\mathrm{tur,in}} \tag{4}$$

$$T_{\mathrm{tur,out}} = T_{\mathrm{tur,in}} / \pi_{\mathrm{tur}}^{(n-1)/n} \tag{5}$$

$$W_{\mathrm{comp}} = G_{\mathrm{air}} c_p (T_{\mathrm{comp,out}} - T_{\mathrm{comp,in}}) \eta_{\mathrm{comp}} \tag{6}$$

The coefficient of performance (*COP*) of the heat pump is defined as the ratio of the heat supplied by the heat pump to the work input consumed during operation:

$$COP = \frac{Q_{ex}}{W_{comp} - W_{tur}} \tag{7}$$

For the working fluid–molten salt heat exchanger of the heat pump, the energy balance equation is

$$Q_{ex} = G_{\text{m-salt}} (h_{\text{m-salt,out}} - h_{\text{m-salt,in}}) = G_{\mathrm{air}} (h_{\mathrm{air,in}} - h_{\mathrm{air,out}}) \eta_{ex} \tag{8}$$

For molten salt thermal energy storage, the energy balance equation of the steam–molten salt heat exchanger is

$$G_{\text{m-salt}}(h_{\text{m-salt,out}} - h_{\text{m-salt,in}}) = G_{\text{steam}}(h_{\text{steam,in}} - h_{\text{steam,out}})\eta_{ex} \quad (9)$$

where $\pi$ denotes the pressure ratio; $n$ denotes the polytropic exponent; $G$ denotes the mass flow rate, in kg/s; $c_p$ denotes the specific heat capacity of air at constant pressure, in J/(kgK); and $\eta_{ex}$ denotes the heat exchanger effectiveness. Based on typical design practice and operational experience, the heat exchanger effectiveness is assumed to be constant at 0.98 under the considered operating conditions; $h$ denotes the specific enthalpy of the working fluid, in kJ/kg; the subscripts air, steam, and m-salt denote the working fluid air, steam, and molten salt, respectively; and the subscripts in and out denote the inlet and outlet of each component, respectively.

The modeling of the coal-fired power generation unit is based on the following major assumptions: the model operates under steady thermodynamic states at different operating conditions, with unsteady effects during load variations neglected, so that the modeling results correspond to a quasi-steady-state model; the unit operates under constant-pressure mode, with the main steam pressure remaining unchanged across all operating conditions; heat losses from heaters and piping are neglected, and the terminal temperature differences in each regenerative heater are specified and remain constant. Apart from extraction steam pressure losses and boiler internal pressure losses, other piping pressure losses are also neglected.

Based on this, the boiler load $Q_b$ can be expressed as follows:

$$Q_b = G_0 h_0 + G_{rh} h_{rh} - G_{fw} h_{fw} - G_{crh} h_{crh} \quad (10)$$

where $G_0$, $G_{rh}$, $G_{crh}$ and $G_{fw}$ are the mass flow rates of main steam, reheat steam, cold reheat steam, and boiler feedwater, respectively, in kg/s; $h_0$, $h_{rh}$, $h_{crh}$ and $h_{fw}$ are the specific enthalpies of main steam, reheat steam, cold reheat steam, and boiler feedwater, respectively, in kJ/kg.

On the steam turbine side, a segmented stage-group model can be established according to the inlet and exhaust steam points as well as the regenerative extraction steam points. The characteristic relationship among stage-group pressure, temperature, and steam mass flow rate is shown in Equation (11):

$$\frac{G_1}{G_N} = \sqrt{\frac{p_1^2 - p_2^2}{p_{1N}^2 - p_{2N}^2}} \cdot \sqrt{\frac{T_{1N}}{T_1}} \quad (11)$$

where $G_1$ is the mass flow rate of the stage group under off-design conditions, in kg/s; $G_N$ is the mass flow rate of the stage group under design conditions, in kg/s; $p_1$ and $p_2$ are the inlet and outlet pressures of the steam turbine stage group under off-design conditions, in MPa; $p_{1N}$ and $p_{2N}$ are the inlet and outlet pressures of the steam turbine stage group under design conditions, in MPa; $T_1$ is the inlet temperature of the steam turbine stage group under off-design conditions, in K; and $T_{1N}$ is the inlet temperature of the steam turbine stage group under design conditions, in K.

The regenerative extraction steam enters the various heaters of the unit, and a matrix model of the heaters can be established through heat balance equations. For the three high-pressure heaters and the deaerator, it can be expressed as

$$\begin{bmatrix} \varphi_1 & & & \\ \lambda_1 & \varphi_2 & & \\ \lambda_2 & \lambda_2 & \varphi_3 & \\ \lambda_3 & \lambda_3 & \lambda_3 & \varphi_4 \end{bmatrix} \begin{bmatrix} \alpha_1 \\ \alpha_2 \\ \alpha_3 \\ \alpha_4 \end{bmatrix} = \begin{bmatrix} \delta_1 \\ \delta_2 \\ \delta_3 \\ \delta_4 \end{bmatrix} \tag{12}$$

For the four low-pressure heaters,

$$\begin{bmatrix} \varphi_5 & & & \\ \lambda_5 & \varphi_6 & & \\ \lambda_6 & \lambda_6 & \varphi_7 & \\ \lambda_7 & \lambda_7 & \lambda_7 & \varphi_8 \end{bmatrix} \begin{bmatrix} \alpha_5 \\ \alpha_6 \\ \alpha_7 \\ \alpha_8 \end{bmatrix} = \left(1 - \sum_{i=1}^{4} \alpha_i\right) \begin{bmatrix} \delta_5 \\ \delta_6 \\ \delta_7 \\ \delta_8 \end{bmatrix} \tag{13}$$

where $\alpha_i$ is the extraction steam coefficient, that is, the ratio of extraction steam to feedwater flow rate; and $\delta_i$, $\varphi_i$, and $\lambda_i$ are the enthalpy changes associated with the inlet and outlet of the regenerative heaters:

$$\delta_i = \alpha_{\text{discharge}} \left(h_{wi} - h_{w(i+1)}\right) \tag{14}$$

$$\varphi_i = h_i - h_{di} \tag{15}$$

$$\lambda_i = h_{di} - h_{d(i+1)} \tag{16}$$

where $\alpha_{\text{discharge}}$ is the diverted feedwater flow rate for molten salt heat release, which needs to be calculated at the appropriate regenerative heater according to the heat release scheme; $h_{wi}$ is the outlet water enthalpy of each stage of the regenerative heaters, in kJ/kg; $h_i$ is the extraction steam enthalpy, in kJ/kg; and $h_{di}$ is the drain enthalpy of each stage of the regenerative heaters, in kJ/kg.

By combining the heat balance matrix with the characteristic relationships among stage-group pressure, temperature, and steam mass flow rate, the operating parameters of the thermal power unit under heat storage and heat release conditions can be calculated. The output power $P_0$ of the entire steam turbine unit can be obtained from the following equation:

$$P_0 = \eta_m \eta_{ai} \left[ G_{fw} \left( h_0 + \alpha_{rh} h_{rh} - \sum_{i=1}^{8} \alpha_i h_i - \alpha_c h_c - \sum \alpha_{charge} h_{charge} \right) \right] / 3600 \tag{17}$$

$$\alpha_c = 1 - \sum_{i=1}^{8} \alpha_i - \sum \alpha_{charge} \tag{18}$$

where $\alpha_c$ and $h_c$ denote the exhaust steam coefficient and exhaust steam enthalpy (kJ/kg), respectively; $h_{wi}$ is the outlet water enthalpy of each stage of the regenerative heaters, in kJ/kg; $\alpha_{charge}$ and $h_{charge}$ denote the heat storage steam coefficient and heat storage steam enthalpy (kJ/kg), respectively; $\eta_m$ is the mechanical efficiency, taken as 0.99; and $\eta_{ai}$ is the generator efficiency, taken as 0.985.

### *3.2. Model Reliability Verification*

To verify the accuracy of the model, it was assumed that the leakage loss from steam turbine shaft seals could be neglected. Three typical operating conditions of a supercritical unit (N600-24.2/566/566) were selected for simulation, namely 100% THA, 75% THA, and 30% THA. The design parameters of the unit were derived from the turbine heat balance diagrams under off-design conditions. A comparison between the simulation results under each operating condition and the design values is shown in Table 2. As can be seen from Table 2, the calculated results of the model are basically consistent with the reference design values. The relative errors of data such as the inlet and outlet pressures, temperatures, and

flow rates of the main steam, first reheat steam, and second reheat steam are all within 4%, and most of the errors are less than 1%. To validate the accuracy of the Brayton heat pump model, simulations were performed using the same working fluid and storage medium as in Ref. [16], and the results were compared with the experimental data therein Table 3. The comparison demonstrates good agreement, confirming the reliability of the proposed model. Therefore, it can be demonstrated that the established mathematical model is accurate and reliable and can meet the needs of the subsequent study.

**Table 2.** Comparison between simulated values and designed values.

| Name/Unit | 100% THA | | | 75% THA | | | 30% THA | | |
|---|---|---|---|---|---|---|---|---|---|
| | Sim. | Des. | Error | Sim. | Des. | Error | Sim. | Des. | Error |
| Power Generation/MW | 598.92 | 600 | 0.18% | 494.15 | 495 | 0.17% | 197.85 | 198.06 | 0.11% |
| Main Steam Pressure/MPa | 24.27 | 24.2 | 0.29% | 24.28 | 24.2 | 0.33% | 24.14 | 24.2 | 0.25% |
| 1st Extraction Pressure/MPa | 5.79 | 5.8 | 0.17% | 4.222 | 4.233 | 0.26% | 1.809 | 1.805 | 0.22% |
| 2nd Extraction Pressure/MPa | 4.12 | 4.11 | 0.24% | 3.043 | 3.038 | 0.16% | 1.313 | 1.316 | 0.23% |
| 3rd Extraction Pressure/MPa | 2.030 | 2.025 | 0.25% | 1.509 | 1.506 | 0.20% | 0.6565 | 0.655 | 0.23% |
| 4th Extraction Pressure/MPa | 1.006 | 1.008 | 0.20% | 0.759 | 0.761 | 0.26% | 0.3203 | 0.321 | 0.22% |
| 5th Extraction Pressure/MPa | 0.326 | 0.32 | 1.88% | 0.3082 | 0.299 | 1.27% | 0.1313 | 0.129 | 1.78% |
| 6th Extraction Pressure/MPa | 0.1258 | 0.127 | 0.94% | 0.09867 | 0.095 | 3.86% | 0.03886 | 0.040 | 2.85% |
| 7th Extraction Pressure/MPa | 0.063 | 0.062 | 1.6% | 0.04612 | 0.047 | 1.87% | 0.02093 | 0.021 | 0.33% |
| 8th Extraction Pressure/kPa | 20.96 | 21 | 0.19% | 15.94 | 16 | 0.38% | 7.99 | 8 | 0.12% |
| Exhaust Pressure/kPa | 4.91 | 4.9 | 0.20% | 4.89 | 4.9 | 0.20% | 4.88 | 4.9 | 0.41% |
| Heat Rate/kJ/(kW·h) | 7512.5 | 7508.3 | 0.06% | 7600.2 | 7589.8 | 0.14% | 8605.2 | 8590.8 | 0.17% |
| Thermal Efficiency | 0.4357 | 0.436 | 0.06% | 0.4307 | 0.4312 | 0.13% | 0.3802 | 0.3809 | 0.18% |

**Table 3.** Parameter comparison for the Brayton heat pump.

| Name/Unit | Ref. | Calc. | Error |
|---|---|---|---|
| Heat Source Inlet Temperature/°C | 270.85 | 270.85 | 0.00% |
| Heat Source Outlet Temperature/°C | 584.35 | 580.07 | −0.73% |
| Cold Source Inlet Temperature/°C | 26.85 | 26.85 | 0.00% |
| Cold Source Outlet Temperature/°C | 8.55 | 10.06 | +17.66% |
| Compressor Inlet Temperature/°C | 21.05 | 20.98 | −0.33% |
| Compressor Outlet Temperature/°C | 589.05 | 589 | −0.01% |
| Expander Inlet Temperature/°C | 287.65 | 295 | +2.56% |
| Expander Outlet Temperature/°C | −31.25 | −31.25 | 0.00% |
| *COP* | 1.2 | 1.19 | −0.83% |

### *3.3. Method for Evaluating Thermodynamic Performance*

For the performance evaluation of the coupled system, the assessment is mainly carried out from three indicators: the system efficiency over the entire process of energy storage and release, peak-regulation capacity, and round-trip efficiency.

The thermal efficiency $\eta$ of the coupled system over the entire process of energy storage and release is

$$\eta = \frac{\int_{t_1}^{t_2} P_{ct}dt + \int_{t_3}^{t_4} P_{st}dt}{\int_{t_1}^{t_2} (Q_{b,ct}/\eta_{bt})dt + \int_{t_3}^{t_4} (Q_{b,st}/\eta_{bt})dt} \times 100\% \quad (19)$$

where $P_{ct}$ is the electric power output of the system during heat storage, in kW; $t_1$ and $t_2$ are the start and end times of the heat storage process, respectively, in h; $P_{st}$ is the electric power output of the system during heat release, in kW; $t_3$ and $t_4$ are the start and end times of the heat release process, respectively, in h; $Q_{b,ct}$ is the boiler thermal load during the heat

storage period, in kW; $Q_{b,st}$ is the boiler thermal load during the heat release period, in kW; $\eta_{bt}$ is the boiler efficiency during the heat storage and release periods.

Peak-regulation capacity reflects the additional range by which the unit can increase or decrease its load after being coupled with the molten salt thermal energy storage system, and it is one of the indicators used to evaluate system flexibility. The peak-regulation capacity $\Delta P_{ct}$ during the energy storage process is

$$\Delta P_{ct} = P_0 - P_{ct} \tag{20}$$

The system peak-regulation capacity $\Delta P_{st}$ during the heat release process is

$$\Delta P_{st} = P_{st} - P_e \tag{21}$$

In order to analyze how effectively the thermal energy storage system converts the stored heat into electrical energy of the generating unit, the round-trip efficiency $\eta_{r,t}$ is defined as the ratio of the increased power generation during the heat release stage to the reduced power generation during the heat storage stage, and its expression is as follows:

$$\eta_{r,t} = \frac{\int_{t_3}^{t_4} \Delta P_{st} dt}{\int_{t_1}^{t_2} \Delta P_{ct} dt} \times 100\% \tag{22}$$

## 4. Results and Analysis

### 4.1. Analysis of Energy Storage Process

During the energy storage process, the coupled system can store energy either through molten salt thermal energy storage or through heat pump cycle-based thermal energy storage. Therefore, the performance of these two energy storage modes, namely molten salt thermal energy storage and heat pump thermal energy storage, was analyzed under three operating conditions: 30% THA, 75% THA, and 100% THA.

Figure 3 shows the load response curves during the heat storage process. In the figure, "without thermal energy storage" represents the time required for the actual power plant, when no thermal energy storage system is used, to reduce its power generation output by 65 MW. The two dashed lines respectively represent the times required for the power plant to reduce its power generation output by 65 MW when molten salt thermal energy storage and heat pump thermal energy storage are employed. It can be seen from the figure that both molten salt thermal energy storage and heat pump thermal energy storage significantly improve the load regulation capability of the unit. Compared with molten salt thermal energy storage, heat pump thermal energy storage exhibits a somewhat faster response in load reduction, mainly because the two systems differ in their energy conversion and transfer mechanisms. Molten salt thermal energy storage converts the reduced electrical energy of the unit into thermal energy through a heat exchanger and stores it in high-temperature molten salt. This process involves a certain degree of thermal inertia and heat transfer delay. In contrast, the heat pump thermal energy storage system uses a reverse Brayton cycle to directly upgrade thermal energy through components such as compressors and expanders. Its power regulation can be rapidly achieved by changing the compressor speed or valve opening, and the circulation velocity of the working fluid and the dynamic response of the system are both faster. Therefore, when it is necessary to reduce power generation output (that is, to draw electricity from the grid for thermal energy storage), heat pump thermal energy storage has a shorter load reduction response time.

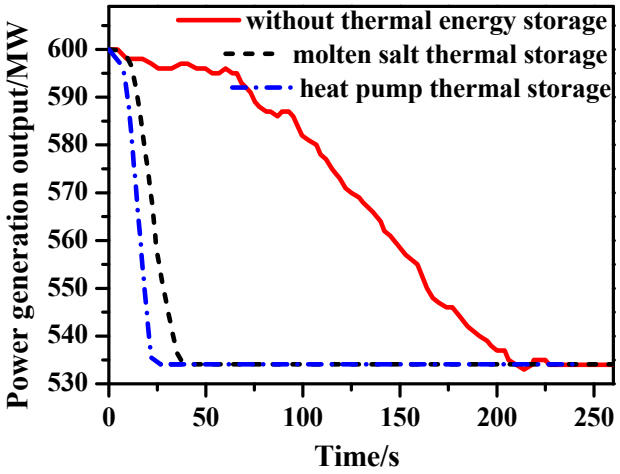


**Figure 3.** Expected load response curve during the energy storage process.

Figure 4 shows the thermal storage loads of molten salt thermal energy storage and heat pump thermal energy storage, respectively, for a thermal power unit coupled with thermal energy storage participating in grid peak regulation under 30% THA, 75% THA, and 100% THA operating conditions when the peak-regulation capacity is reduced. It can be seen from the figure that, under the same peak-regulation capacity, the thermal energy storage capacity of molten salt thermal energy storage is greater than that of heat pump thermal energy storage. The reason is that molten salt thermal energy storage achieves a reduction in power generation by extracting reheat steam to heat the molten salt, thereby reducing the steam's ability to conduct work as its thermal energy is removed. Since the power generation efficiency of thermal power units is about 35–45%, reducing power generation by 1 MW requires extracting approximately 2.2–2.8 MW of heat from the steam. By contrast, heat pump thermal energy storage consumes auxiliary power to drive the compressor and is limited by the coefficient of performance (*COP*) of the heat pump, so consuming 1 MW of electrical power can only generate about 1.7 MW of thermal energy. Therefore, for the same unit reduction in power generation, the corresponding thermal energy storage amount of molten salt thermal energy storage is greater than that of heat pump thermal energy storage. In addition, when the same peak-regulation capacity is reduced, the thermal energy storage amount of molten salt thermal energy storage increases with increasing THA operating condition, whereas that of heat pump thermal energy storage does not vary with the THA operating condition. The reason is that, at low load (30% THA), the steam consumption rate of the steam turbine is high and the electricity generated per kilogram of steam is low, so less steam mass flow needs to be extracted to reduce the same amount of power generation, and the temperature and pressure of that steam are also lower, resulting naturally in less total heat being transferred after heat exchange with the molten salt. At high load (75% and 100% THA), the steam consumption rate is lower and the steam has a stronger ability to conduct work, so more steam must be extracted to reduce the same amount of power generation, and the steam parameters are also higher, causing the heat obtained by the molten salt to increase accordingly. Therefore, the thermal energy storage amount of molten salt thermal energy storage increases with increasing THA. In contrast, the heat pump thermal energy storage system is electrically and thermally decoupled from the steam turbine thermodynamic cycle, and its thermal energy storage amount depends on the electrical power consumed, which is determined by the peak-regulation command, rather than on the current THA operating condition of the steam turbine. Therefore, regardless of whether the unit is operating at 30%, 75%, or 100% THA, the thermal energy storage amount of heat pump thermal energy storage under the same peak-regulation capacity remains almost completely the same. This difference makes

molten salt thermal energy storage more suitable for deep coupling with thermal power generation under high-load, high-quality steam conditions, whereas heat pump thermal energy storage offers greater deployment flexibility and operational independence over the full load range, especially during low-load periods of deep peak regulation.

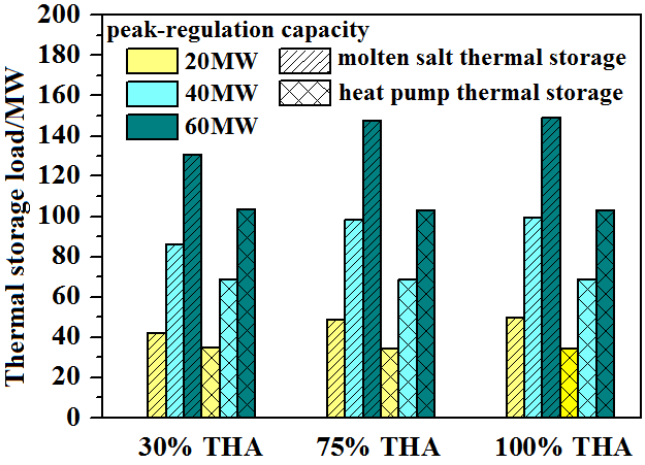


**Figure 4.** Comparative analysis of thermal energy storage capacity during the energy storage process.

### *4.2. Analysis of Energy Release Process*

Figure 5 shows the load response curve during the heat release process. In the figure, "without thermal energy storage" represents the time required for the actual power plant, without using a thermal energy storage system, to increase its power output by 50 MW through increased boiler firing. Scheme 1 represents the time required for the power output to increase by 50 MW during the heat release process in which stored thermal energy replaces extraction steam from the four low-pressure stages. Scheme 2 represents the time required for the power output to increase by 50 MW in the process where stored thermal energy is used to heat part of the feedwater extracted from the intermediate tap of the feedwater pump, generating steam that is then introduced into the intermediate-pressure cylinder to conduct work and increase the power output of the intermediate- and low-pressure cylinders. Scheme 3 represents the time required for the power output to increase by 50 MW during the heat release process in which stored thermal energy replaces extraction steam from the three high-pressure stages. It can be seen from the figure that the release of heat from the thermal energy storage system can significantly shorten the time required for the unit to raise its load during peak regulation. It can also be observed that Scheme 3 has a higher rate of increase in power output than Scheme 1, while Scheme 2 has the lowest rate of increase in power output among the three schemes. The reasons are as follows: Scheme 3 responds the fastest because it directly displaces the extraction steam from the three high-pressure stages of the unit. Once the stored thermal energy is put into use, more high-grade steam is allowed to return to the high-pressure cylinder to conduct work, resulting in the most rapid rise in power output. Scheme 1 ranks second because it replaces extraction steam from the four low-pressure stages, where the steam pressure is low and the specific volume is large, so the decrease in extraction steam flow is relatively gradual and the rise in power output is slightly slower. Scheme 2 is the slowest, and the core reason lies in its heat transfer and flow characteristics: the stored heat must raise the feedwater temperature from about 190 °C to 560 °C, and under the condition of fixed heat release on the molten salt side, the large heat transfer temperature difference forces the feedwater flow rate to fall to an extremely low level. Although this correspondingly reduces the feedwater flow passing through the high-pressure heaters, thereby lowering the extraction steam flow from the three stages to some extent, Scheme 2 does not essentially

suppress the unit's extraction steam directly. Instead, it adds a new steam source for doing work that has high parameters but extremely low flow rate and a slow establishment of flow, and therefore its increase in power output is the slowest.

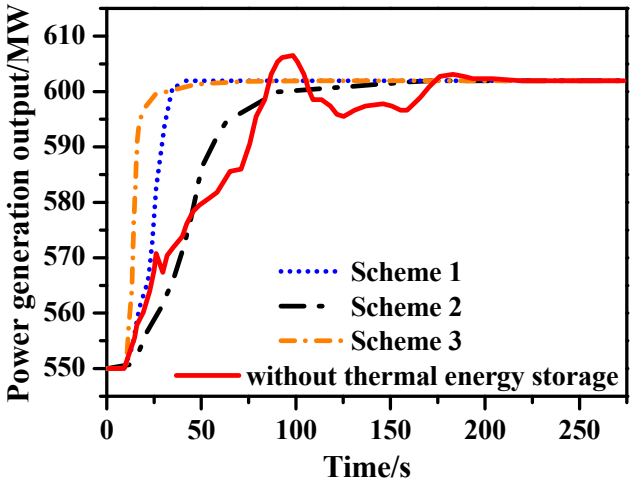


**Figure 5.** Expected load response curve during the heat release process.

Figure 6 is a comparative analysis of the increased power output (peak-regulation capacity) provided by different thermal energy storage modes and heat release schemes when the thermal energy storage system is in the energy release stage. It can be seen from the figure that, during heat release, Scheme 3 increases power output more than Scheme 2, while Scheme 2 increases power output more than Scheme 1. This is because the differences in power generation increment among the three schemes stem from differences in the "grade" of thermal energy substitution and the "work-producing path". In Scheme 1, the replaced low-pressure extraction steam originally has very limited work-producing capability, and the steam saved mainly expands in the low-pressure cylinder, so the marginal increase in power generation is limited. In Scheme 2, the stored heat is used to generate intermediate-pressure steam, which directly increases the steam flow through the intermediate-pressure cylinder and thereby simultaneously raises the power output of both the intermediate- and low-pressure cylinders. Therefore, its power increment is higher than that of Scheme 1 by about 13–19%. In Scheme 3, the replaced steam is high-pressure extraction steam, which has the greatest work-producing capability. After being replaced by stored heat, the saved high-pressure steam can continue to expand through the high-, intermediate-, and low-pressure cylinders over the entire expansion process, so the increase in power generation is more than 50% higher than that of Scheme 2. This reflects the thermodynamic principle that the higher the extraction steam pressure, the greater the benefit after replacement. In addition, under the same heat release scheme, molten salt thermal energy storage produces a greater increase in power output during energy release than heat pump thermal energy storage. This is because, during the energy storage stage, molten salt thermal energy storage actually stores more heat. Although heat pump thermal energy storage can achieve heat upgrading through the heat pump, its net stored heat is lower under the same "thermal energy storage capacity" design because it is constrained by the compressor, the thermal storage medium, and the temperature difference across the heat exchanger. During energy release, even if the heat-to-power conversion paths of the two modes are exactly the same, the one with the greater initial stored heat will inevitably deliver higher power output. Quantitatively, the heat released by molten salt thermal energy storage is about 1.3–1.4 times that of heat pump thermal energy storage.

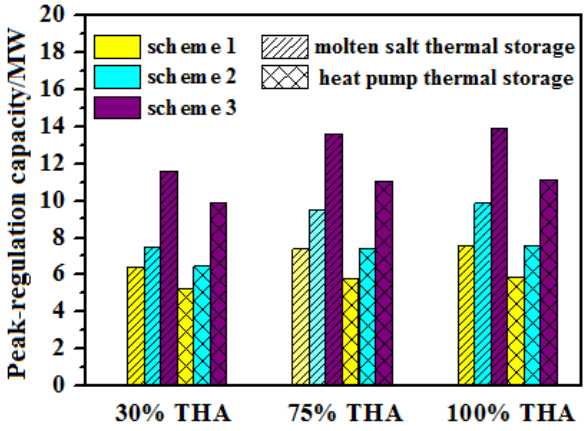


(**a**) 20 MW

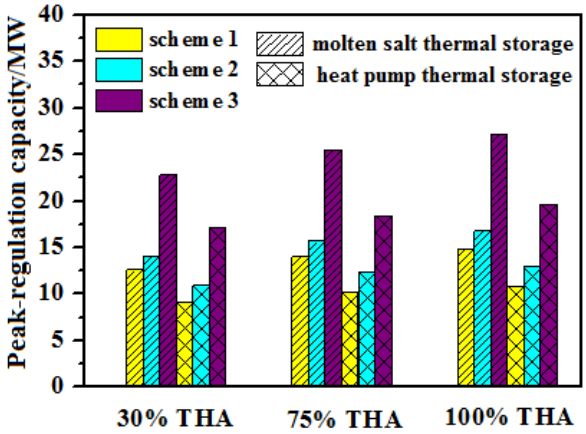


(**b**) 40 MW

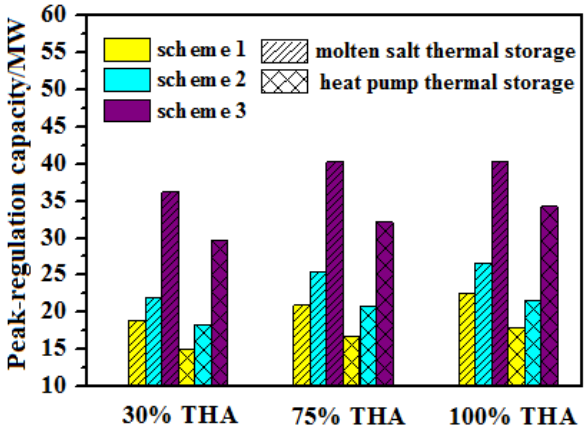


(**c**) 60 MW

**Figure 6.** Comparative analysis of peak-regulation capacity during energy release.

### *4.3. Analysis of the Entire Energy Storage and Release Process*

Figure 7 presents the analysis of the thermal efficiency of the coupled system over the entire process of energy storage and release. By comparison with the parameters in Table 2, it can be seen that the thermal efficiency of the coupled thermal energy storage system is lower than that of the system without thermal energy storage, and as the heat storage and heat release loads increase, the thermal efficiency of the system gradually decreases. This is because the energy storage system itself also involves unavoidable thermal losses. Although molten salt thermal energy storage and heat pump thermal energy storage differ in their heat storage principles, during the heat release stage, both must transfer heat to the steam through heat exchangers, and temperature-difference losses are therefore

unavoidable; moreover, the greater the amount of stored heat, the greater the loss. In fact, the participation of the energy storage system cannot improve the thermal efficiency of the thermal power unit and instead causes the thermal efficiency of the coupled thermal power unit to decline. However, coupling with an energy storage system is an important means of overcoming the temporal and spatial limitations of energy transfer in conventional coal-fired generating units and enhancing their peak-regulation flexibility. The addition of a thermal energy storage system can significantly improve peak-regulation performance at the cost of only a small loss in efficiency.

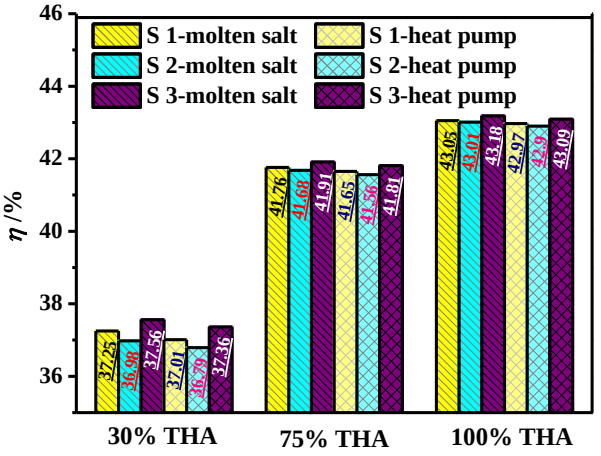


(**a**) 20 MW

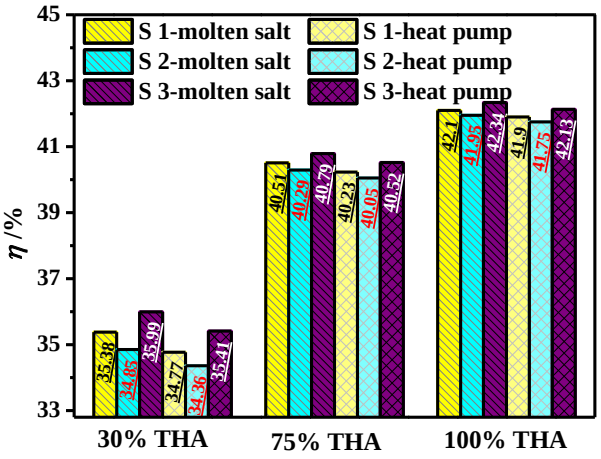


(**b**) 40 MW

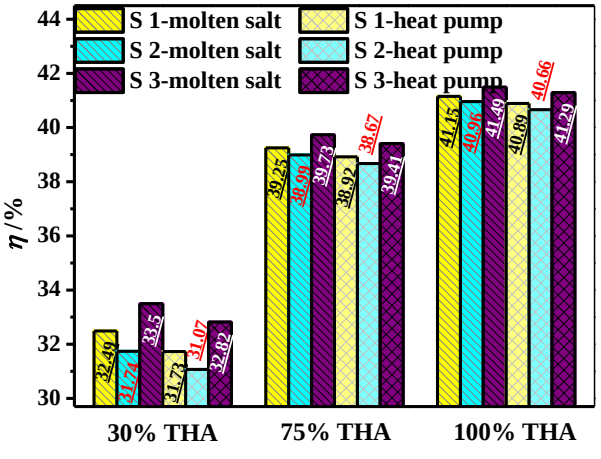


(**c**) 60 MW

**Figure 7.** Thermal efficiency of the coupled system over the entire energy storage and release process.

A comparison of Figure 7 also shows that the thermal efficiency over the entire energy storage and release process differs under different energy storage modes and different energy release schemes. A comparison of the three energy release schemes indicates that Scheme 3 has the highest thermal efficiency, followed by Scheme 1, while Scheme 2 has the lowest. The reason why Scheme 3 achieves the highest efficiency is that the stored heat replaces the extraction steam from the three high-pressure stages, which is characterized by high pressure and high temperature. This portion of extraction steam originally possesses a very high work-producing potential. After being replaced by stored thermal energy, the saved high-pressure steam can continue expanding from the inlet of the high-pressure cylinder all the way to the condenser, resulting in the longest work-producing path and thus the greatest power generation output per unit of heat. Scheme 1 ranks in the middle in terms of efficiency because it replaces the extraction steam from the four low-pressure stages, which is at a lower pressure. The saved steam mainly performs work in the low-pressure cylinder, so the work-producing path is shorter, and the exergy value of the low-pressure extraction steam itself is relatively low; therefore, its thermal efficiency is lower than that of Scheme 3. Scheme 2 has the lowest efficiency because, in this scheme, the stored heat must first be used to heat feedwater to generate steam, which is then introduced into the intermediate-pressure cylinder. During this process, there are heat transfer losses, as well as throttling or mixing losses, when the steam is introduced; the response time is relatively slow; and the temperature grade of the heat declines during transmission, resulting in the greatest exergy loss. Therefore, although the peak-regulation capacity (increase in power generation) of Scheme 2 lies between that of Scheme 1 and Scheme 3, its thermal efficiency is lower than that of Scheme 1. This clearly demonstrates that a "larger peak-regulation capacity" does not necessarily mean a "higher thermal efficiency"—the latter depends more on the magnitude of exergy loss during the heat conversion process.

In addition, regarding the efficiency differences under different THA operating conditions, the order is 100% THA > 75% THA > 30% THA. The fundamental reason is that the intrinsic efficiency of the steam turbine decreases as the load declines. Under the low-load condition of 30% THA, the overall steam parameters are lower than those under high-load conditions. In essence, the energy storage and release system "inserts" the stored heat back into the system, and the equivalent work-producing potential corresponding to this portion of heat is inherently lower under low-load conditions than under high-load conditions. Therefore, regardless of which energy release mode is adopted, the overall thermal efficiency over the entire process under low-load conditions is inevitably lower than that under high-load conditions.

Figure 8 presents an analysis of the round-trip efficiency during the energy storage and release process. Round-trip efficiency reflects the degree of completeness of energy conversion during the storage and release process. It can be seen from the figure that, under the same conditions, the round-trip efficiency under the 100% THA condition is greater than that under the 75% THA condition, which in turn is greater than that under the 30% THA condition. The round-trip efficiency under the 75% THA condition is about 12–15% higher than that under the 30% THA condition, while that under the 100% THA condition is about 1–3.5% higher than that under the 75% THA condition. The reason is that, under low-load conditions, the extraction steam parameters at each stage of the steam turbine decrease and the internal efficiency declines, so the "electrical energy equivalent" corresponding to steam extraction or heat pump heating during the energy storage stage is higher, while the increment in power generation that can be produced by the same amount of heat during the energy release stage is smaller. Under high-load conditions, the unit operates in a high-efficiency region, allowing the stored thermal energy to be converted into

electrical energy more fully. Therefore, the round-trip efficiency increases monotonically with increasing load.

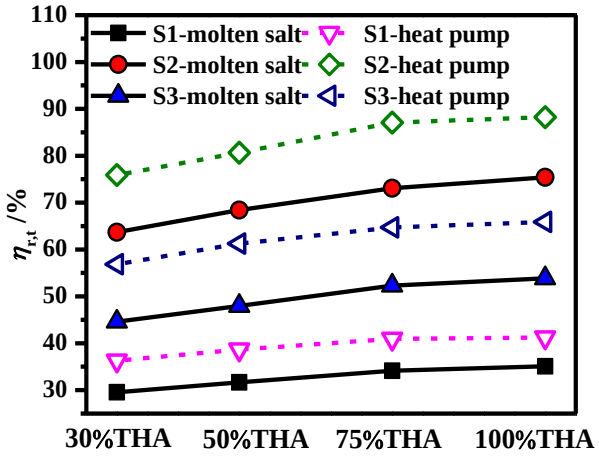


(**a**) 20 MW

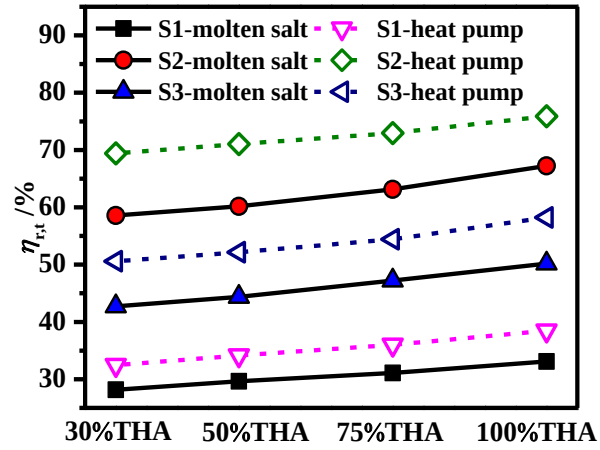


(**b**) 40 MW

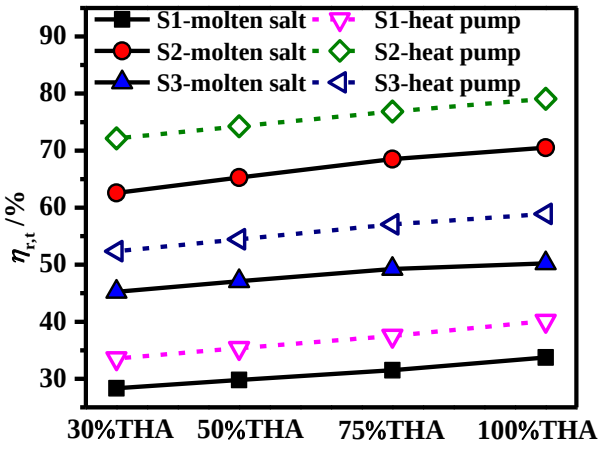


(**c**) 60 MW

**Figure 8.** Round-trip efficiency of the coupled system during the energy storage and release process.

Under the same energy release scheme, the round-trip efficiency of heat pump thermal energy storage is significantly higher than that of molten salt thermal energy storage. Taking the case of 100% THA, 20 MW, and Scheme 2 as an example, the round-trip efficiency of heat pump thermal energy storage is 85.24%, while that of molten salt thermal energy

storage is 75.39%; that is, the round-trip efficiency of heat pump thermal energy storage is about 10% higher than that of molten salt thermal energy storage. The reason is that heat pump thermal energy storage uses the heat pump cycle to "transport" heat from the environment or waste heat, so that, for the same reduction in power generation output, the required energy storage time is shorter and the total electricity consumed during the energy storage stage is smaller. In other words, the "denominator" of round-trip efficiency is significantly smaller than that of molten salt thermal energy storage.

In addition, among the three energy release schemes, Scheme 2 (generating steam and introducing it into the intermediate-pressure cylinder) has the highest round-trip efficiency, followed by Scheme 3 (replacing high-pressure extraction steam), while Scheme 1 (replacing low-pressure extraction steam) has the lowest. This ranking is not the same as that of thermal efficiency and needs to be analyzed in conjunction with peak-regulation capacity and load response time. Although Scheme 2 has relatively low thermal efficiency during energy release, it features a long energy release duration and a moderate increase in peak-regulation capacity, thereby forming a characteristic of "slow increase and steady return," which results in the highest round-trip efficiency. Scheme 3 has the largest increment in peak-regulation capacity during energy release, but because its energy release duration is also relatively short, its overall energy return capability is not strong, and its round-trip efficiency is therefore lower than that of Scheme 2. In Scheme 1, the increment in peak-regulation capacity during energy release is too small and the energy release duration is also relatively short, leading to the lowest degree of energy return. Therefore, Scheme 2 obtains more electrical energy through its return characteristic of "slow release and low-amplitude increase".

The integration of molten salt and heat pump storage with coal-fired power plants has been proven to improve peak-shaving capability. In terms of financial returns, the core economic rationale lies in storing thermal energy in molten salt during off-peak periods using low-cost electricity to drive heat pumps or electric heaters, and subsequently releasing the stored heat for power generation or heating during peak-price periods. Although the present study does not include a detailed economic assessment, the proposed scheme combining molten salt storage with heat pump and extraction steam heating demonstrates strong technical and policy-level feasibility.

## 5. Conclusions

This study retrofitted a thermal power plant for flexible peak-shaving using molten salt and heat pump thermal energy storage. The peak-shaving capacity, thermal efficiency, and round-trip efficiency of both storage modes were investigated under various discharge schemes. The detailed comparative conclusions are as follows:

(1) During load-reduction peak-shaving processes, the heat pump storage system exhibits a relatively fast response in load reduction, making it suitable for rapid load-following scenarios. In contrast, the molten salt storage system responds more slowly due to thermal inertia and heat exchange lag. However, under the same peak-shaving capacity, molten salt storage provides greater thermal storage capacity, which increases with rising THA conditions, whereas the storage capacity of the heat pump system remains largely independent of THA. This indicates that molten salt storage possesses superior thermal regulation potential under high-load conditions.

(2) The discharge strategy significantly influences both peak-shaving capacity and round-trip efficiency. In terms of peak-shaving capacity, Scheme S3 (replacing high-pressure extraction steam) achieves a maximum of 40.2 MW, which is 78% higher than that of Scheme S2 (introducing generated steam into the intermediate-pressure cylinder) at its maximum of 22.5 MW, while Scheme S1 (replacing low-pressure extraction steam)

ranks in between with a maximum of 26.6 MW. Regarding overall thermal efficiency across all THA conditions, the ranking is consistently S3 > S1 > S2. However, the ranking for round-trip efficiency differs, with S2 > S3 > S1, indicating that Scheme S2 achieves the highest electricity recovery rate through its "slow-release, low-power" return characteristic. Under the same discharge scheme, the power output from molten salt storage is approximately 1.3 to 1.4 times that of heat pump storage.

(3) The integration of thermal energy storage systems achieves a substantial enhancement in peak-shaving flexibility at the expense of a marginal thermal efficiency penalty. Although the thermal efficiency of the coal-fired unit slightly decreases due to heat exchange temperature difference losses, this trade-off constitutes a critical enabler for operational flexibility, providing a viable technical pathway for the flexibility retrofitting of thermal power plants under high-penetration renewable energy grid integration.

**Author Contributions:** L.C.: Conceptualization, Funding acquisition, Supervision; J.X.: Data curation, Software, Writing—original draft, Writing—review & editing; F.H.: Formal analysis, Writing—review & editing; P.L.: Software, Writing—original draft, Writing—review & editing. All authors have read and agreed to the published version of the manuscript.

**Funding:** This research was funded by National Natural Science Foundation of China, grant number 52176003.

**Data Availability Statement:** The data presented in this study are available on request from the corresponding author.

**Acknowledgments:** The authors are grateful for the support from the National Natural Science Foundation of China (Grant numbers 52176003).

**Conflicts of Interest:** The authors declare that they have no known competing financial interests or personal relationships that could have appeared to influence the work reported in this paper.

## Nomenclature

Roman letters

| | |
|---|---|
| $c_p$ | Specific heat capacity [J/(kg·K)] |
| $G$ | Mass flow rate [kg/s] |
| $h$ | Specific enthalpy [kJ/kg] |
| $P$ | Output power [MW] |
| $Q$ | Load [MW] |
| $T$ | Temperature [K] |

Greek letters

| | |
|---|---|
| $\alpha_c$ | Exhaust steam coefficient [-] |
| $\alpha_{charge}$ | Heat storage steam coefficient [-] |
| $\alpha_{\mathrm{discharge}}$ | Diverted feedwater flow rate for molten salt heat release |
| $\alpha_i$ | Extraction steam coefficient [-] |
| $\eta_{ai}$ | Generator efficiency [-] |
| $\eta_{\mathrm{b}}$ | Boiler efficiency [-] |
| $\eta_m$ | Mechanical efficiency [-] |
| $\eta_{r,t}$ | Ratio of the increased power generation to the reduced power generation |
| $\lambda$ | Thermal conductivity [W/(m·K)] |
| $\mu$ | Viscosity [Pa·s] |
| $\rho$ | Density [kg/m$^3$] |
| $\delta_i$ | Enthalpy changes associated with the inlet of the regenerative heaters [kJ/kg] |
| $\varphi_{\mathrm{i}}$ | Enthalpy changes associated with the onset of the regenerative heaters [kJ/kg] |

Subscripts and abbreviations

| | |
|---|---|
| COP | Coefficient of performance |
| MSHE | Molten salt heat exchanger |
| THA | Turbine heat acceptance |
| TES | Thermal energy storage |
| crh | Cold reheat steam |
| ct | Heat storage period |
| di | Drain |
| fw | Boiler feedwater |
| st | Heat release period |

## References


1. Zhang, Z.G.; Kang, C.Q. Challenges and prospects for constructing the new-type power system towards a carbon neutrality future. *Proc. CSEE* **2022**, *42*, 2806–2819. [CrossRef]
2. Chen, Y.S.; Bian, G.L.; Gong, J.G. Revenue analysis and evaluation of wind-solar-thermal coupled systems in the context of peak regulation auxiliary service market. *Distrib. Gener. Altern. Energy J.* **2024**, *39*, 941–960. [CrossRef]
3. Mallapaty, S. How China could be carbon neutral by mid-century. *Nature* **2020**, *586*, 482–483. [CrossRef] [PubMed]
4. Blanquiceth, J.; Cardemil, J.; Henríquez, M.; Escobar, R. Thermodynamic evaluation of a pumped thermal electricity storage system integrated with large-scale thermal power plants. *Renew. Sustain. Energy Rev.* **2023**, *175*, 113134. [CrossRef]
5. Jia, T.L.; Shuai, Y.; Wang, F.Q.; Zhang, H.; Yang, D.Z.; Geng, B.X.; Li, Q.Y.; Wu, Q.Y.; Xu, Y. Empowering modern power systems with thermal energy storage in China: A comprehensive review. *Renew. Sustain. Energy Rev.* **2026**, *235*, 116937. [CrossRef]
6. Li, B.; Cao, Y.; He, T.Y.; Si, F. Thermodynamic analysis and operation strategy optimization of coupled molten salt energy storage system for coal-fired power plant. *Appl. Therm. Eng.* **2024**, *236*, 121702. [CrossRef]
7. Song, K.; Hou, T.Z.; Jiang, J.H.; Grigoriev, S.A.; Fan, F.L.; Qin, J.; Wang, Z.X.; Sun, C.Y. Thermal management of liquid-cooled proton exchange membrane fuel cell: A review. *J. Power Sources* **2025**, *648*, 237227. [CrossRef]
8. Ma, T.S.; Li, Z.K.; Lv, K.; Chang, D.; Hu, W.; Zou, Y. Design and performance analysis of deep peak shaving scheme for thermal power units based on high temperature molten salt heat storage system. *Energy* **2024**, *288*, 129557. [CrossRef]
9. Li, L.; Li, W.Y.; Ma, J.L. Research on coordinated control strategy of power response rate of thermal power plant with high temperature molten salt heat storage. *Int. J. Heat Technol.* **2023**, *41*, 55–62. [CrossRef]
10. Lin, X.J.; Sun, P.; Zhong, W.; Wang, J. Thermodynamic analysis and operation investigation of a cross-border integrated energy system based on steam Carnot battery. *Appl. Therm. Eng.* **2023**, *220*, 119804. [CrossRef]
11. Wei, H.J.; Lu, Y.W.; Yang, Y.C.; Zhang, C.; He, C.; Wu, Y.; Li, W.; Zhao, D. Research on influence of steam extraction parameters and operation load on operational flexibility of coal fired power plant. *Appl. Therm. Eng.* **2021**, *195*, 117226. [CrossRef]
12. Wang, B.G.; Ma, H.; Ren, S.J.; Si, F. Effects of integration mode of the molten salt heat storage system and its hot storage temperature on the flexibility of a subcritical coal-fired power plant. *J. Energy Storage* **2023**, *58*, 106410. [CrossRef]
13. Richter, M.; Oeljeklaus, G.; Görner, K. Improving the load flexibility of coal-fired power plants by the integration of a thermal energy storage. *Appl. Energy* **2019**, *236*, 607–621. [CrossRef]
14. Abbas, S.; Hassan, A.; Zhou, J.; Bisengimana, E.; Yousuf, S.; Hassan, M.; Yuan, Y. Progress and challenges in the integration of solar heat pumps with thermal collectors and PCM-based thermal energy storage systems for heating applications. *Sol. Energy* **2025**, *301*, 113919. [CrossRef]
15. Zhang, X.; Sun, Y.; Zhao, W.L.; Li, C.; Xu, C.; Sun, H.; Yang, Q.; Tian, X.; Wang, D. The Carnot batteries thermally assisted by the steam extracted from thermal power plants: A thermodynamic analysis and performance evaluation. *Energy Convers. Manag.* **2023**, *297*, 117724. [CrossRef]
16. Salomone-González, D.; González-Ayala, J.; Medina, A.; Roco, J.; Curto-Risso, P.; Hernández, A.C. Pumped heat energy storage with liquid media: Thermodynamic assessment by a Brayton-like model. *Energy Convers. Manag.* **2020**, *226*, 113540. [CrossRef]
17. Wang, H.C.; Han, J.B.; Zhang, R.Y.; Sun, M.; Sun, Z.; Hua, P.; Xie, Z.; Wang, H.; Abdollahi, E.; Lahdelma, R.; et al. Heat-power peak shaving and wind power accommodation of combined heat and power plant with thermal energy storage and electric heat pump. *Energy Convers. Manag.* **2023**, *297*, 117732. [CrossRef]
18. Yu, B.X.; Han, R.; Liu, Q.; Liao, Z.; Xu, C. Thermodynamic performance of a flexible retrofit Carnot battery energy storage system in a coupled thermal power plant. *Energy Storage Sci. Technol.* **2025**, *14*, 1461–1470. [CrossRef]
19. Janz, G.J.; Tomkins, R.P.T. *Physical Properties Data Compilations Relevant to Energy Storage. IV. Molten Salts: Data on Additional Single and Multicomponent Salt Systems*; National Institute of Standards and Technology: Gaithersburg, MD, USA, 1981.

20. Wang, C.; Hu, Y.; He, Y. Optical, thermal, and structural performance analyses of a parabolic-trough solar collector. *J. Renew. Sustain. Energy* **2020**, *12*, 053704. [CrossRef]
21. Xin, Q.R.; Wang, J.L.; Jian, M.; Li, Z.W.; Ivan, T.; Daryn, K.; Bai, X.H.; Sun, C.Y. Comprehensive performance analysis and optimization of the closed Brayton cycle for waste heat recovery and cooling in hydrogen aeroengines. *Energy* **2026**, *349*, 140647. [CrossRef]